Available online at www.sciencedirect.com
ScienceDirect
Journal of Sound and Vibration 319 (2009) 260–281
JOURNAL OF SOUND AND VIBRATION
www.elsevier.com/locate/jsvi

Semi-analytical study of free vibration characteristics of shear deformable filament wound anisotropic shells of revolution

Altan Kayran*, Erdem Yavuzbalkan

Department of Aerospace Engineering, Middle East Technical University, 06531 Ankara, Turkey

Received 19 July 2007; received in revised form 5 May 2008; accepted 20 May 2008
Handling Editor: C.L. Morfey
Available online 9 July 2008

Abstract

Free vibration characteristics of filament wound anisotropic shells of revolution are investigated by using multisegment numerical integration technique in combination with a modified frequency trial method. The applicability of multisegment numerical integration technique is extended to the solution of free vibration problem of anisotropic composite shells of revolution through the use of finite exponential Fourier transform of the fundamental shell equations. The governing shell equations comprise the full anisotropic form of the constitutive relations, including first-order transverse shear deformation, and all components of translatory and rotary inertia. The variation of the stiffness coefficients along the axis of the shell is also incorporated into the solution method. Filaments are assumed to be placed along the geodesic fiber path on the shell of revolution resulting in the variation of the stiffness coefficients along the axis of the composite shell of revolution with general meridional curvature. Sample solutions have been performed on the effect of the variation of the stiffness coefficients on the free vibration behavior of filament wound truncated conical and spherical shells of revolution.

1. Introduction

Laminated composite structures are finding ever increasing application areas in many engineering disciplines due to their superior strength to weight, stiffness to weight ratio and corrosion-resistant properties, among others, compared to structures made of metallic isotropic materials. A shell of revolution is a widely encountered structure in many applications such as pressure vessels, rocket nozzles, fuselage frames, external stores, antenna, etc. Laminated shells in which each layer can have arbitrary fiber orientation are macroscopically anisotropic, and these structures show coupling effect between various modes of deformation such as extension, bending, and twisting. Anisotropy significantly complicates the equations governing the free vibration problem of general shells of revolution, and the governing equations describing the symmetric and antisymmetric responses, with respect to circumferential coordinate, associated with each Fourier harmonic are coupled.

*Corresponding author. Tel.: +90 312 2104274; fax: +90 312 2104250.
E-mail address: akayran@metu.edu.tr (A. Kayran).

0022-460X/$ - see front matter © 2008 Elsevier Ltd. All rights reserved.
doi:10.1016/j.jsv.2008.05.024

Accurate prediction of the dynamic response characteristic of shells made from advanced composites requires the use of refined theories. These theories predominantly account for transverse shear deformation, which is neglected in classical laminated shell theory. Low ratio of the transverse shear modulus to the in-plane modulus accounts for the more important role that transverse shear deformation plays in reducing the effective flexural stiffness of shells made from composites than metallic shells. Noor and Burton [1] have made an assessment of computational models used for multilayered composite shells, and addressed the significance of the transverse shear deformation for accurate prediction of the response of multilayered shells.

Several solution strategies have been used for the vibration analysis of laminated composite shells of revolution. The most commonly used approach is based on the representation of the shell variables by a Fourier series in the circumferential coordinate combined with the use of a numerical discretization technique such as finite elements, finite differences or numerical integration in the meridional direction.

Some examples of these studies include the work of Noor and Peters [2], who used a combination of Fourier series representation in the circumferential direction, and three-field mixed finite element model for the discretization in the meridional direction. Ganesan and Sivadas [3] studied the vibration of anisotropic cylindrical and conical shells using a semi-analytical finite element method, in which circumferential variation of variables is represented by a double Fourier series with finite element discretization in the meridional direction. Sheinman and Weissman [4] studied the coupling between symmetric and antisymmetric modes in anisotropic shells using conical finite elements and classical shell theory in which transverse shear deformation effects are not taken into account. A semi-analytical study of the composite shells of revolution has been performed by Xi et al. [5], who used a similar solution technique like Sheinman, but also included transverse shear deformation in their analysis. A finite element semi-analytical model for laminated axisymmetric shells is presented by Pinto Correia et al. [6]. In their study, shell is modeled by a series of conical finite elements in the meridional direction, similar to the treatment of Sheinman and Weissman [4] and Xi et al. [5], but they have utilized a higher-order displacement field to account for the thickness effect, which becomes more important in the analysis of interlaminar shear stresses and transverse normal stresses.

Heylinger and Jilani [7] incorporated Ritz method using a combination of power and Fourier series as the approximating functions for three displacement components for the solution of vibration problem of anisotropic shells. Tan [8] presented an efficient substructuring analysis method for predicting the natural frequencies of shells of revolution utilizing the Sturm sequence method in conjunction with the massive substructuring technique. The solution procedure was capable of handling general type of material property, and any kind of boundary condition. Tımarcı and Soldatos [9] used the state space concept on the Love-type version of a unified shear deformable shell theory, to study the axisymmetric and flexural vibrations of angle-ply laminated circular cylindrical shells.

The present study aims at achieving two main goals. The first goal is to give a detailed description of the extension of the application of multisegment numerical integration technique [10] to the solution of free vibration problem of anisotropic shells of revolution. This extension is achieved through the use of finite exponential Fourier transform of the fundamental shell equations. Solution procedure is based on a modified frequency trial method, which processes on the numerically integrated transformed fundamental system of equations of anisotropic shells of revolution. Fundamental system of shell equations are derived such that the full anisotropic form of the constitutive relations, including first-order transverse shear deformation, and all components of translatory and rotary inertia are included in the analysis. The solution methodology, which is explained in detail in the present paper, has also been successfully applied to the free vibration analysis of anisotropic branched shells of revolution with ring stiffeners by Kayran and Yavuzbalkan [11]. In Ref. [11], the authors have applied the solution method to constant thickness branched shells of revolution by assuming that the composite layers have constant fiber orientation along the shell axis. Such an assumption results in constant stiffness coefficients along the axis of the shell of revolution.

The second goal of the present study is to incorporate the arbitrary variation of the stiffness coefficients along the axis of the shell of revolution into the solution method. It is known that in case of arbitrary orientation of the fibers with respect to the geometric axis of the shell, which is typical in filament winding operation, the stiffness coefficients vary along the axis of the shells of revolution with general meridional curvature or conical shells [12]. In the current study, the composite shell of revolution is assumed to be produced by the filament winding operation, and the filaments are assumed to be placed along geodesic fiber

path on the shell of revolution resulting in variation of the stiffness coefficients along the meridian of the shell of revolution. Semi-analytical solution method is extended to include the arbitrary variation of the stiffness coefficients along the axis of the shell, and the effect of variation of the stiffness coefficients on the free vibration characteristics is investigated for general shells of revolution. Sample results have been obtained for filament wound truncated conical and spherical shells of revolution.

2. Fundamental system of equations of anisotropic shells of revolution

In the following, the fundamental system of equations will be presented for a general shell of revolution. Fig. 1 shows the geometry notation used. In Fig. 1, R_θ and R_ϕ denote the radii of curvature of the middle surface of the shell in the tangential (θ) and meridional (ϕ) directions, respectively. R denotes the distance of the shell mid surface from the axis of revolution ($R = R_\theta \sin\phi$). In accordance with the first-order transverse shear deformation theory, the displacement field is approximated as in

$$U_\phi(\phi,\theta,\zeta,t) = u_\phi^0(\phi,\theta,t) + \zeta\beta_\phi(\phi,\theta,t) \tag{1}$$

$$U_\theta(\phi,\theta,\zeta,t) = u_\theta^0(\phi,\theta,t) + \zeta\beta_\theta(\phi,\theta,t) \tag{2}$$

$$W(\phi,\theta,\zeta,t) = w^0(\phi,\theta,t) \tag{3}$$

where U_ϕ, U_θ, W represent the displacement of a general point in the shell thickness in meridional, tangential and thickness directions, respectively. In Eqs. (1)–(3), $u_\phi^0, u_\theta^0, w^0$ represent the mid surface displacements at the reference surface $\zeta = 0$, and β_ϕ and β_θ represent the rotations of a transverse normal about θ and ϕ curvilinear coordinates, respectively.

The starting point in the application of numerical integration technique for the solution of vibration problem of a shell of revolution is to express the equations governing the free vibration as a system of partial differential equations given in the form of Eq. (4). Fundamental system of equations given by Eq. (4) are obtained by deriving expressions for the first derivative of the fundamental shell variables with respect to meridional coordinate ϕ

$$\frac{\mathrm{d}\boldsymbol{\psi}(\phi,\theta)}{\mathrm{d}\phi} = f\left(\boldsymbol{\psi}(\phi,\theta), \frac{\partial}{\partial\theta}(\boldsymbol{\psi}(\phi,\theta)), \frac{\partial^2}{\partial^2\theta}(\boldsymbol{\psi}(\phi,\theta))\right) \tag{4}$$

In Eq. (4), $\boldsymbol{\psi}$ is a vector representing the fundamental shell variables that enter into the appropriate boundary conditions on a rotationally symmetric edge of the shell of revolution, and for the Reissner–Naghdi

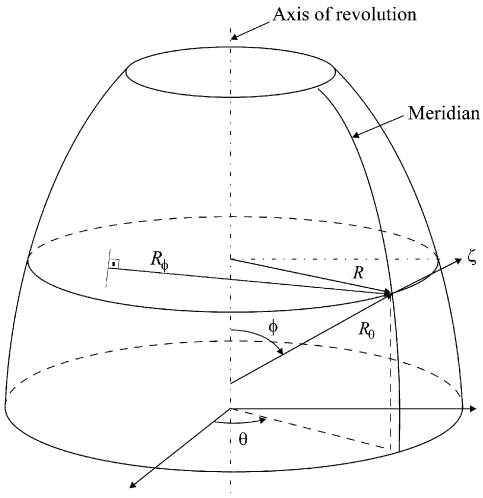

Fig. 1. Geometry and coordinate system of the shell of revolution.

improved shell theory they are given by

$$\boldsymbol{\psi}(\phi,\theta,t)=\left[w^0,u^0_\phi,u^0_\theta,\beta_\phi,\beta_\theta,Q_\phi,N_{\phi\phi},N_{\phi\theta},M_{\phi\phi},M_{\phi\theta}\right]^{\mathrm{T}} \tag{5}$$

The unknown variables in Eq. (5) are called as the fundamental variables, and the first half consists of the reference plane displacements and the second half consist of the stress and moment resultants which are defined in appropriate manner [13–15].

The system of equations given by Eq. (4) is derived by the complex manipulation of three sets of equations which are the strain displacement relations of the Reissner–Naghdi shell theory [16], dynamic equilibrium equations [13,15], and full anisotropic form of the constitutive relations relating the stress and moment resultants to reference surface strains $\left(\varepsilon^0_{\phi\phi},\varepsilon^0_{\theta\theta},\gamma^0_{\phi\theta}\right)$ and curvatures $(\kappa_{\phi\phi},\kappa_{\theta\theta},\kappa_{\phi\theta})$ of the laminated shell wall. For a laminated shell wall, the constitutive relations relating the stress and moment resultants to reference surface strains and curvatures are given in matrix form [14]

$$\begin{bmatrix}N_{\phi\phi}\\N_{\theta\theta}\\N_{\phi\theta}\\M_{\phi\phi}\\M_{\theta\theta}\\M_{\phi\theta}\end{bmatrix}=\begin{bmatrix}A_{11}&A_{12}&A_{16}&B_{11}&B_{12}&B_{16}\\A_{12}&A_{22}&A_{26}&B_{12}&B_{22}&B_{26}\\A_{16}&A_{26}&A_{66}&B_{16}&B_{26}&B_{66}\\B_{11}&B_{12}&B_{16}&D_{11}&D_{12}&D_{16}\\B_{12}&B_{22}&B_{26}&D_{12}&D_{22}&D_{26}\\B_{16}&B_{26}&B_{66}&D_{16}&D_{26}&D_{66}\end{bmatrix}\begin{bmatrix}\varepsilon^0_{\phi\phi}\\\varepsilon^0_{\theta\theta}\\\gamma^0_{\phi\theta}\\\kappa_{\phi\phi}\\\kappa_{\theta\theta}\\\kappa_{\phi\theta}\end{bmatrix} \tag{6}$$

In Eq. (6) N_{ij} terms represent force per unit length, and M_{ij} terms represent moment per unit length. The stiffness coefficients are expressed in the usual manner [14].

Integration of the transverse shear stresses across the thickness of the shell yields the transverse shear stress resultants as in

$$\begin{bmatrix}Q_\theta\\Q_\phi\end{bmatrix}=\begin{bmatrix}As_{44}&As_{45}\\As_{45}&As_{55}\end{bmatrix}\begin{bmatrix}\gamma^0_\theta\\\gamma^0_\phi\end{bmatrix} \tag{7}$$

In Eq. (7) the transverse shear stiffness coefficients are given by

$$(As_{44},As_{45},As_{55})=\sum_{k=1}^{N_L}\int_{h_{k-1}}^{h_k}\left(\bar{Q}^{(k)}_{44},\bar{Q}^{(k)}_{45},\bar{Q}^{(k)}_{55}\right)f(\zeta)\,\mathrm{d}\zeta$$
$$f(\zeta)=\frac{5}{4}\left[1-4\left(\frac{\zeta}{h}\right)^2\right] \tag{8}$$

In Eq. (8), it is assumed that the transverse shear stress has a parabolic distribution across the shell wall. A factor of 5/4 multiplies the distribution function used by Whitney [17] so that the shear factor calculated for the layered anisotropic shell wall can be consistent with the established shear factor from the previous work of Reissner [16] and Mindlin [18] for the homogenous case.

The derivation of the fundamental system of equations, for anisotropic shells of revolution, in the form of Eq. (4) is explained in detail by Yavuzbalkan [19]. Because of the full anisotropic form of the constitutive relations, the derivation process is rather lengthy and symbolic algebra is utilized to derive the fundamental system of equations in the form of Eq. (4).

In the derivation process of dynamic equilibrium equations, application of Hamilton's principle also generates conditions on the boundary displacements, and boundary stress and moment resultants which are applied at the constant meridional coordinate ($\phi=$ constant) of a shell of revolution. For the free vibration problem, boundary conditions are given by setting one of the variables, given inside the parenthesis of the shell variable pairs in Eq. (9), to zero [13]

$$(N_{\phi\phi},u^0_\phi),(N_{\phi\theta},u^0_\theta),(Q_\phi,w^0),(M_{\phi\phi},\beta_\phi),(M_{\phi\theta},\beta_\theta)=0 \tag{9}$$

For anisotropic shells of revolution, which are characterized by the constitutive relations given by Eqs. (6) and (7), the existence of full coupling stiffness coefficients precludes the uncoupling of fundamental system of shell equations, describing the symmetric and antisymmetric responses with respect to circumferential coordinate, by the classical Sine or Cosine Fourier decomposition of the fundamental shell variables. Therefore, to accomplish the uncoupling of the circumferential coordinate from the fundamental system of equations, each fundamental variable is expanded in complex Fourier series as shown in Eq. (10). This process is essentially equivalent to expanding each fundamental variable in Fourier series with Sine and Cosine terms in the circumferential direction

$$\boldsymbol{\psi}(\phi,\theta)=\sum_{-\infty}^{+\infty}\boldsymbol{\psi}_n(\phi)\mathrm{e}^{\mathrm{i}n\theta} \tag{10}$$

$$\boldsymbol{\psi}_n(\phi)=\frac{1}{2\pi}\int_0^{2\pi}\boldsymbol{\psi}(\phi,\theta)\mathrm{e}^{-\mathrm{i}n\theta}=\boldsymbol{\psi}_{nc}(\phi)-i\boldsymbol{\psi}_{ns}(\phi) \tag{11}$$

where

$$\boldsymbol{\psi}_{nc}(\phi)=\frac{1}{2\pi}\int_0^{2\pi}\boldsymbol{\psi}(\phi,\theta)\cos n\theta\,\mathrm{d}\theta \tag{12}$$

$$\boldsymbol{\psi}_{ns}(\phi)=\frac{1}{2\pi}\int_0^{2\pi}\boldsymbol{\psi}(\phi,\theta)\sin n\theta\,\mathrm{d}\theta \tag{13}$$

It is clearly seen in Eq. (11) that application of finite exponential Fourier transform results in doubling of the number of fundamental variables. In this study, conversion of the system of partial differential equations, Eq. (4), to a system of ordinary differential equations is accomplished through the use of finite exponential transform given by Eq. (11).

Application of the finite exponential Fourier transform to Eq. (4) results in a system of 20 first-order ordinary differential equations, which is represented by the matrix equation

$$\frac{\mathrm{d}\boldsymbol{\psi}}{\mathrm{d}\phi}=\frac{\mathrm{d}}{\mathrm{d}\phi}\begin{bmatrix}\boldsymbol{\psi}^{(1)}(\phi)\\ \boldsymbol{\psi}^{(2)}(\phi)\end{bmatrix}=\mathbf{K}(n,\omega,\phi)\begin{bmatrix}\boldsymbol{\psi}^{(1)}(\phi)\\ \boldsymbol{\psi}^{(2)}(\phi)\end{bmatrix} \tag{14}$$

In Eq. (14) n is the circumferential wave number, ω is the natural frequency and partitions of the fundamental variable vector are given by

$$\boldsymbol{\psi}^{(1)}(\phi)=\left[w^0_{nc},w^0_{ns},u^0_{\phi nc},u^0_{\phi ns},u^0_{\theta nc},u^0_{\theta ns},\beta_{\phi nc},\beta_{\phi ns},\beta_{\theta nc},\beta_{\theta ns}\right]^{\mathrm{T}} \tag{15}$$

$$\boldsymbol{\psi}^{(2)}(\phi)=\left[Q_{\phi nc},Q_{\phi ns},N_{\phi\phi nc},N_{\phi\phi ns},N_{\phi\theta nc},N_{\phi\theta ns},M_{\phi\phi nc},M_{\phi\phi ns},M_{\phi\theta nc},M_{\phi\theta ns}\right]^{\mathrm{T}} \tag{16}$$

In Eqs. (15) and (16), displacement and stress and moment resultants with subscript 'c' refer to symmetric modes with respect to the tangential coordinate θ of the shell of revolution, and subscript 's' refers to antisymmetric modes. The elements of the coefficient matrix $\mathbf{K}$ are given in Appendix A in detail.

3. Method of solution

The solution of Eq. (14) together with the transformed boundary conditions for the natural frequencies and the transformed displacements, and stress and moment resultants, is performed by the multisegment numerical integration technique. However, due to the application of finite exponential Fourier transform to handle the full anisotropic form of the constitutive relations, eigenvalue extraction process differs from the technique proposed by Kalnins [10].

In the multisegment numerical integration technique, the shell is divided into M number of segments in the meridional direction, and the solution to Eq. (14) can be written as

$$\boldsymbol{\psi}(\phi)=\mathbf{T}_i(n,\omega,\phi)\boldsymbol{\psi}(\phi_i)\quad(i=1,2,\ldots,M) \tag{17}$$

Transfer matrices $\mathbf{T}_i$ are obtained from the initial value problems defined in each segment i by Eq. (18) subject to initial conditions given by Eq. (19). In Eq. (19) $\mathbf{I}$ is the identity matrix

$$\frac{\mathrm{d}\mathbf{T}_i(n,\omega,\phi)}{\mathrm{d}\phi} = \mathbf{K}(n,\omega,\phi)\mathbf{T}_i(n,\omega,\phi) \tag{18}$$

$$\mathbf{T}_i(n,\omega,\phi_i) = \mathbf{I} \tag{19}$$

Continuity requirements of the fundamental variables at the end points of the segments lead from Eq. (17) to the partitioned matrix equation:

$$\begin{bmatrix} \boldsymbol{\psi}^{(1)}(\phi_{i+1}) \\ \boldsymbol{\psi}^{(2)}(\phi_{i+1}) \end{bmatrix} = \begin{bmatrix} \mathbf{T}^{(1)}(\phi_{i+1}) & \mathbf{T}^{(2)}(\phi_{i+1}) \\ \mathbf{T}^{(3)}(\phi_{i+1}) & \mathbf{T}^{(4)}(\phi_{i+1}) \end{bmatrix}_i \begin{bmatrix} \boldsymbol{\psi}^{(1)}(\phi_i) \\ \boldsymbol{\psi}^{(2)}(\phi_i) \end{bmatrix} \quad (i = 1,2,\ldots,M) \tag{20}$$

When the boundary conditions given by Eq. (9) are transformed, a total of ten elements of the fundamental variable vector $\boldsymbol{\psi}$ at each edge of the shell, ϕ_1 and ϕ_{M+1}, must be prescribed. For computational ease, the rows of the fundamental variable vector $\boldsymbol{\psi}$ at both ends of the shell, ϕ_1 and ϕ_{M+1}, are adjusted such that the first ten elements of $\boldsymbol{\psi}(\phi_1)$ and the last ten elements of $\boldsymbol{\psi}(\phi_{M+1})$ are the prescribed boundary conditions. In the following, to keep the uniformity of the notation used for the partitioned fundamental variable vector, the boundary conditions are also represented by the same vector notation defined by Eqs. (15) and (16). Therefore, boundary conditions at the ends of the shell of revolution are expressed by

$$\boldsymbol{\psi}^{(1)}(\phi_1) = \boldsymbol{\psi}^{(2)}(\phi_{M+1}) = 0 \tag{21}$$

Eq. (20) constitutes a system of linear homogenous matrix equation with $2M$ unknowns. The solution for the eigenvalue problem requires the writing out of matrix equations in each interval i separately, and bringing the whole equation set into an upper diagonal matrix equation by Gauss elimination. The resulting matrix equation is given by

$$\begin{bmatrix} \mathbf{E}_1 & -\mathbf{I} & 0 & . & . & 0 \\ 0 & \mathbf{C}_1 & -\mathbf{I} & 0 & . & 0 \\ . & 0 & . & . & . & . \\ . & . & 0 & . & . & . \\ 0 & . & . & 0 & \mathbf{E}_M & -\mathbf{I} \\ 0 & . & . & 0 & 0 & \mathbf{C}_M \end{bmatrix} \begin{bmatrix} \boldsymbol{\psi}^{(2)}(\phi_1) \\ \boldsymbol{\psi}^{(1)}(\phi_2) \\ . \\ . \\ \boldsymbol{\psi}^{(2)}(\phi_M) \\ \boldsymbol{\psi}^{(1)}(\phi_{M+1}) \end{bmatrix} = 0 \tag{22}$$

where the (10×10) matrices $\mathbf{E}_i$ and $\mathbf{C}_i$ are evaluated successively from

$$\mathbf{E}_1 = \mathbf{T}_1^{(2)} \tag{23}$$

$$\mathbf{C}_1 = \mathbf{T}_1^{(4)}\mathbf{E}_1^{-1} \tag{24}$$

$$\mathbf{E}_i = \mathbf{T}_i^{(2)} + \mathbf{T}_i^{(1)}\mathbf{C}_{i-1}^{-1} \quad (i = 2,3,\ldots,M) \tag{25}$$

$$\mathbf{C}_i = \left(\mathbf{T}_i^{(4)} + \mathbf{T}_i^{(3)}\mathbf{C}_{i-1}^{-1}\right)\mathbf{E}_i^{-1} \quad (i = 2,3,\ldots,M) \tag{26}$$

Natural frequencies are determined by requiring non-trivial solution of the last row of Eq. (22), and setting the determinant of the coefficient matrix to zero

$$\det \mathbf{C}_M = 0 \tag{27}$$

Assuming that a particular natural frequency is determined from Eq. (27), then from the last row of Eq. (22), $\boldsymbol{\psi}^{(1)}(\phi_{M+1})$ is determined up to an arbitrary constant. The remaining unknown fundamental variables at each end of the shell segments can then be calculated successively from

$$\boldsymbol{\psi}^{(2)}(\phi_M) = \mathbf{E}_M^{-1}\boldsymbol{\psi}^{(1)}(\phi_{M+1}) \tag{28}$$

$$\boldsymbol{\psi}^{(1)}(\phi_{M-i+1}) = \mathbf{C}_{M-i}^{-1}\boldsymbol{\psi}^{(2)}(\phi_{M-i+1}) \quad (i = 1, 2, \ldots, M-1) \tag{29}$$

$$\boldsymbol{\psi}^{(2)}(\phi_{M-i}) = \mathbf{E}_{M-i}^{-1}\boldsymbol{\psi}^{(1)}(\phi_{M-i+1}) \quad (i = 1, 2, \ldots, M-1) \tag{30}$$

For the specially orthotropic material model and improved shell theory, which includes first-order shear deformation, the order of the characteristic matrix $\mathbf{C}_M$ is five [20]. However, the derivation process for the characteristic matrix shows that, for the macroscopically anisotropic material model and first-order shear deformation theory, the order of the characteristic matrix $\mathbf{C}_M$ becomes ten.

The solution of natural frequencies through Eq. (27) requires a frequency search within a given frequency interval. In the present study, the initial value problems defined by Eqs. (18) and (19) are solved by numerically integrating the equations by the IMSL subroutine DIVPAG utilizing the Adams–Moulton numerical integration option. IMSL subroutine DIVPAG uses a user-supplied subroutine where all the elements of the coefficient matrix $\mathbf{K}$ are given. Therefore, as long as the discrete or continuous variation of the elements of the coefficient matrix $\mathbf{K}$, which also includes the stiffness coefficients, along the meridian of the shell is coded accordingly, meridional variation of the shell properties can be handled easily. It is known that in case of filament winding operation, the stiffness coefficients vary along the axis of the shells of revolution with general meridional curvature or conical shells [12]. In this study, the variation of the stiffness coefficients of filament wound shells of revolution is incorporated into the semi-analytical solution process by coding the elements of the coefficient matrix $\mathbf{K}$ accordingly.

The present study revealed that when the fundamental system of equations is obtained by the application finite exponential Fourier transform to the circumferentially coupled partial differential equations, the determinant of the characteristic matrix $\mathbf{C}_M$ was seen not to change sign at the natural frequency. It was observed that when the finite exponential Fourier transform of the fundamental system of partial differential equations were used, the determinant always remained positive, and vanished at natural frequency irrespective of the shell geometry or the constitutive model used. This behavior is studied by looking at the variation of the determinant of the characteristic matrix $\mathbf{C}_M$ for an isotropic cylindrical shell using two different solution approaches. The cylindrical shell investigated for this purpose is an aluminum shell (Young's modulus: 70 GPa, Poisson's ratio: 0.33, density: 2700 kg m^{-3}) with both ends simply supported. The length of the shell is taken as 0.508 m with a thickness of 1.27 mm, and radius of 0.254 m. In the first approach, classical Fourier decomposition is applied to the fundamental shell variables along the circumference, and the governing shell equations are reduced to a system of ten first-order differential equations. In this case each fundamental variable is expanded either in cosine or in sine series in the circumferential direction. Therefore, the system of equations for this case can be directly obtained from Eq. (14) by picking out the fundamental variable vector as in

$$\boldsymbol{\psi}(\phi) = \left[w_{nc}^0, u_{\phi nc}^0, u_{\theta ns}^0, \beta_{\phi nc}, \beta_{\theta ns}, Q_{\phi nc}, N_{\phi\phi nc}, N_{\phi\theta ns}, M_{\phi\phi nc}, M_{\phi\theta ns}\right]^{\mathrm{T}} \tag{31}$$

Thus, total number of fundamental variables is now ten, and the order of the characteristic matrix $\mathbf{C}_M$ is five. The determinant of the characteristic matrix $\mathbf{C}_M$ versus the scaled non-dimensional frequency is plotted in Fig. 2, in a range where a natural frequency actually resides. The non-dimensional frequency is evaluated from

$$\Omega = \omega h\sqrt{\rho/E_1} \tag{32}$$

In Eq. (32), ρ is the mass density, h is the wall thickness of the shell and E_1 is the modulus in the fiber direction for a unidirectional composite or Young's modulus for an isotropic material. In this case, natural frequency is determined by means of inverse interpolation once a sign change in the determinant of the characteristic matrix is detected, and the scaled non-dimensional frequency is determined as 2.986×10^{-3}.

In the second approach, the same problem is formulated by applying finite exponential Fourier transform to the fundamental system of partial differential equations, and the natural frequency is again determined from Eq. (27). In this case, the determinant of the characteristic matrix $\mathbf{C}_M$ versus the scaled non-dimensional frequency is plotted in Fig. 3. It is seen that determinant of the characteristic matrix does not change sign, but rather it is always positive, and vanishes at natural frequency. The determinant values calculated by both approaches are compared in Table 1. It is seen that the determinant of the 10×10 characteristic matrix of the second approach, is exactly the square of the determinant of the 5×5 characteristic matrix of the first

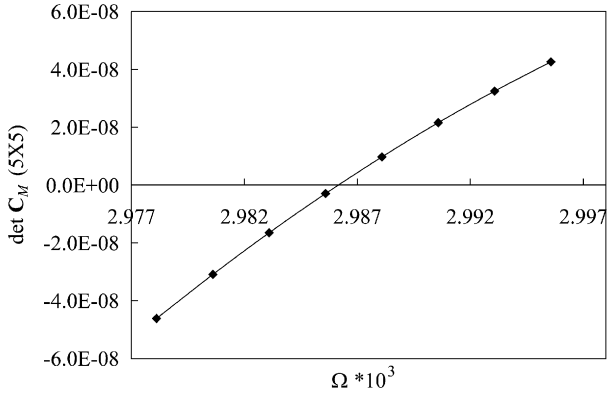

Fig. 2. Determinant of the characteristic matrix: classical Fourier decomposition ($n = 1$).

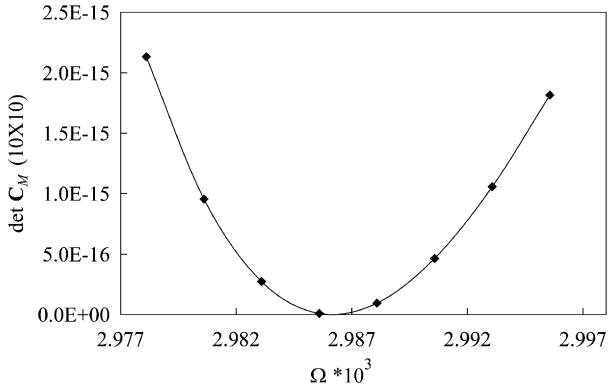

Fig. 3. Determinant of the characteristic matrix: finite exponential transform ($n = 1$).

Table 1
Comparison of characteristic determinants at discrete frequencies

$\Omega*10^3$	Determinant of 5×5 matrix-Fourier decomposition	Determinant of 10×10 matrix-Exponential transform
2.978	−4.618E−08	2.133E−15
2.980	−3.093E−08	9.564E−16
2.983	−1.652E−08	2.729E−16
2.986	−2.969E−09	8.816E−18
2.988	9.723E−09	9.453E−17
2.990	2.155E−08	4.646E−16
2.993	3.252E−08	1.058E−15
2.996	4.262E−08	1.816E−15

approach. Thus, this proves why in the second approach, the determinant versus frequency curve does not change sign when passing through the natural frequency.

The square relation can be proven for any generic two-point boundary value problem by performing the whole numerical integration based solution process, which is described above, symbolically. Yavuzbalkan [19] has proved the square relation for a generic two-point boundary value problem with two dependent and two independent variables, by performing all the calculations symbolically in Matlab. Since the generality of the

solution is not destroyed, the coefficient matrix is taken as constant. Both boundary value problems, which are formulated by the classical Fourier decomposition and finite exponential Fourier transform, are assumed to define an eigenvalue problem, and the solution procedure outlined for the multisegment shell is applied to a single shell segment without loss of generality.

Because the determinant of the characteristics matrix does not change sign through a natural frequency, a different algorithm is employed to locate the natural frequency. The method essentially relies on checking the slope change of the determinant of the characteristic matrix, and detecting the interval where a natural frequency resides. The eigenvalue extraction algorithm designed performs the following tasks.

- slope change detection of the determinant of the characteristic matrix to locate an interval where a natural frequency resides,
- application of inverse interpolation to determine the natural frequency,
- simultaneous check of the gradient of the determinant between successive inverse interpolations to eliminate the possibility detecting a false natural frequency.

The slope change detection algorithm was used to determine the natural frequency of the isotropic cylindrical shell described above, and the scaled non-dimensional natural frequency was again found to be 2.986×10^{-3}. It was seen that the non-dimensional frequencies determined by both the approaches agreed very well. Based on the solution procedure outlined, a computer code is developed which determines the natural frequencies, and the variation of all the fundamental shell variables of laminated anisotropic shells of revolution at each frequency. After the extraction of the natural frequency, the transformed fundamental shell variables (Eqs. (12) and (13)) along the meridian of the shell are determined recursively from Eqs. (28)–(30) by operating on the already determined submatrices $\mathbf{C}_i$ and $\mathbf{E}_i$. The dominant fundamental variable involved in the particular natural vibration mode is decided by looking at the normalized mode shapes along the meridian of the shell. For the particular circumferential wave number, the actual variation of the fundamental variables can be constructed by utilizing the cosine and sine parts of the fundamental shell variables, in the complex Fourier series representation equations (10) and (11).

With the main solution steps outlined in this study, applicability of the multisegment numerical integration technique is extended to the free vibration solution of laminated, shear deformable anisotropic shells of revolution including the variation of the stiffness coefficients along the meridian of the shell.

4. Validation study

For comparison purposes, analysis of an anisotropic shell is performed for a simply supported cylindrical shell geometry which was studied by Noor and Peters [2]. The shell studied has the following material and geometric properties.

Modulus in the fiber direction: $E_1 = 213.74\,\text{GPa}$, Modulus transverse to fiber: $E_2 = 18.62\,\text{GPa}$;
Shear moduli: $G_{12} = G_{13} = 5.171\,\text{GPa}$, $G_{23} = 4.137\,\text{GPa}$, Poisson's ratio: $v = 0.28$;
Mass density: $\rho = 2051.88\,\text{kg}\,\text{m}^{-3}$;
Shell length, L: 0.8 m, shell radius, R: 6.302 cm, total shell thickness, h: 0.508 mm;
Two-layered shell with fiber orientation: $90^\circ/45^\circ$, equal ply thicknesses.

Noor's analytical formulation was based on a form of the Sanders–Budiansky shell theory including the effects of both the transverse shear deformation, and the laminated anisotropic material response. Lowest natural frequencies for circumferential wave numbers ranging from $n = 0$ to 8 are obtained, and the comparison of the results of the present study and the study by Noor and Peters [2] is given in Table 2. Comparison in Table 2 was made based on the non-dimensional frequency parameter given by Noor and Peters [2], $\bar{\omega} = \omega\sqrt{\rho R^2/E_2}$. The results show that most of the non-dimensional frequency parameters agree very well up to the fourth digit.

Table 2
Comparison of natural frequencies

n	Solution by Noor and Peters [2] $\bar{\omega}$	Present solution $\bar{\omega}$
0	0.3087	0.3087
1	0.0444	0.0444
2	0.0161	0.0162
3	0.0328	0.0328
4	0.0621	0.0620
5	0.0991	0.0990
6	0.1443	0.1442
7	0.1978	0.1976
8	0.2618	0.2624

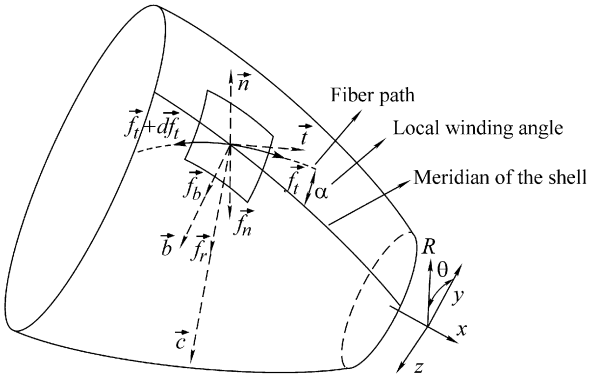

Fig. 4. Fiber path on the surface of a general shell of revolution.

5. Variation of stiffness coefficients for a filament wound shell of revolution

The geometry and winding patterns are the basic parameters governing the manufacturing of a filament wound shell of revolution. In filament winding operation, common way to place filaments is along the geodesic fiber path on the shell of revolution. Geodesic path connects two points along the shortest distance on the surface of a shell of revolution. Placement of fibers along the geodesic paths results in a stable system, and hence no friction is required to keep the fiber from slipping. Fig. 4 shows a typical fiber path on the surface of a shell of revolution. On the surface of the shell of revolution, which is defined by $\vec{S}(x,\theta)$, fiber follows a path $\vec{\Gamma}(s)$

$$\vec{S}(x,\theta) = x\hat{\varepsilon}_1 + R(x)\cos\,\theta\hat{\varepsilon}_2 + R(x)\sin\,\theta\hat{\varepsilon}_3 \tag{33}$$

$$\vec{\Gamma}(s) = x(s)\hat{\varepsilon}_1 + \theta(s)\hat{\varepsilon}_\theta \tag{34}$$

In Eqs. (33) and (34) $\hat{\varepsilon}_1, \hat{\varepsilon}_2, \hat{\varepsilon}_3$ represent the unit vectors in the x, y and z directions, and $\hat{\varepsilon}_\theta$ represent the unit vector in the tangential direction θ. The change in the fiber tension $\vec{f}_t$ along the fiber path gives rise to a force $\vec{f}_r$ given by

$$\vec{f}_r = \frac{\mathrm{d}\vec{f}_t}{\mathrm{d}s} \tag{35}$$

$\vec{f}_r$ is directed towards the center of curvature of the fiber path, and it can be split into a normal component $\vec{f}_n$, which is perpendicular to the surface of the shell of revolution, and a transverse force $\vec{f}_b$ which lies in the tangent plane drawn to the surface. $\vec{f}_b$ is perpendicular to the plane formed by the tangent vector to the fiber path $\vec{t}$ and the normal vector $\vec{n}$. The slippage tendency λ is then defined as the ratio of the transverse force $\vec{f}_b$

and normal force $\vec{f}_n$ [21]

$$\lambda = \frac{\vec{f}_r \cdot \vec{b}}{\vec{f}_r \cdot \vec{n}} = \frac{\vec{c} \cdot \vec{b}}{-\vec{c} \cdot \vec{n}} \tag{36}$$

In Eq. (36) $\vec{c}$ is the unit curvature vector, and $\vec{b}$ is the binormal vector and they are defined by

$$\vec{c} = \frac{\mathrm{d}\vec{t}}{\mathrm{d}s}, \quad \vec{b} = \vec{t} \times \vec{n} \tag{37}$$

and

$$\vec{t} = \frac{\mathrm{d}\vec{S}}{\mathrm{d}s}, \quad \vec{n} = -\vec{S}_x \times \vec{S}_\theta \tag{38}$$

where $\vec{S}_x$ and $\vec{S}_\theta$ are the normalized basis vectors of the surface in the x and θ directions, respectively, and they are given by

$$\vec{S}_x = \frac{1}{\left|\partial\vec{S}/\partial x\right|}\frac{\partial\vec{S}}{\partial x}, \quad \vec{S}_\theta = \frac{1}{\left|\partial\vec{S}/\partial\theta\right|}\frac{\partial\vec{S}}{\partial\theta} \tag{39}$$

The tangent vector to the fiber path can also be written as in

$$\vec{t} = \vec{S}_x \cos\alpha + \vec{S}_\theta \sin\alpha \tag{40}$$

In Eq. (40) α is the local winding angle shown in Fig. 4.

Eq. (36) can be manipulated and brought into the form given by Eq. (41) with the help of Eqs. (37)–(40). A detailed derivation of Eq. (41) can be found in Ref. [21]

$$\frac{\mathrm{d}\alpha}{\mathrm{d}x} = \frac{\lambda((1+R'^2)\sin^2\alpha - RR''\cos^2\alpha) - (1+R'^2)R'\sin\alpha}{R(1+R'^2)\cos\alpha} \tag{41}$$

In Eq. (41) R' indicates the derivative of R with respect to x, and Eq. (41) gives the variation of the winding angle along the axis of the shell of revolution. Since the slippage tendency λ is taken as non-zero, Eq. (41) gives the winding pattern for a non-geodesic fiber path on the surface of the shell of revolution.

For a geodesic fiber path, slippage tendency λ can be taken as zero. In that case for a shell of revolution, Eq. (41) simplifies to Eq. (42)

$$\frac{\mathrm{d}\alpha}{\mathrm{d}x} = \frac{-R'}{R}\tan\alpha \tag{42}$$

For a general shell of revolution, Eq. (42) can be integrated from a known winding angle at one end of the shell of revolution, and the winding angle at any axial location can be calculated for the entire surface of the shell of revolution.

For a truncated conical shell with the cone angle β, integrating equation (42) from a known winding angle β at the smaller end (x_1,R_1) to any axial location (x,R) yields Eq. (43) for the variation of the winding angle along the axis of the conical shell

$$\sin\alpha = \sin\alpha_1\frac{x_1}{x} = \sin\alpha_1\frac{R_1}{R} \tag{43}$$

Eq. (44) gives the identical relation for the variation of the winding angle as in Ref. [12].

For a truncated spherical shell of revolution, integration of Eq. (42) from a known winding angle α_1 at the smaller end ϕ_1 to any meridional location ϕ shown in Fig. 1, and noting that for a spherical shell $R_\phi = R_\theta = R_{\mathrm{sphere}}$ and $R = R_{\mathrm{sphere}}\sin\phi$, gives Eq. (44) for the variation of the winding angle with respect to meridional coordinate ϕ

$$\sin\alpha = \sin\alpha_1\frac{\sin\phi_1}{\sin\phi} \tag{44}$$

In filament winding operation, any unit length of the fiber at any location of the surface of the shell brings with itself the same amount of matrix, and the number of fibers in a cross-section is always constant. Thus, it follows that the thickness at any axial location of a general shell of revolution can be calculated from [12,21]

$$t = t_1 \frac{R_1 \cos \alpha_1}{R \cos \alpha} \tag{45}$$

In Eq. (45), t represents the thickness of a single ply at the axial location where the radius is R, and t_1 represents the thickness of a single ply at the smaller end of the shell of revolution where the radius is R_1.

Eqs. (42) and (45) directly affect the calculation of the stiffness coefficients given by Eqs. (6) and (7), which are calculated in the usual manner [14]. Therefore, for a filament wound shell of revolution, the stiffness coefficients and the thickness of the shell of revolution vary continuously along the meridian of the shell, and these variations are automatically reflected in the elements of the coefficient matrix **K** of Eq. (18). During the numerical integration of the initial value problems, defined by Eqs. (18) and (19) by the IMSL subroutine DIVPAG, all the elements of the coefficient matrix **K** are given in a user-supplied subroutine. In the present study, continuous variation of the stiffness coefficients and thickness for a filament wound shell of revolution are coded in accordance with Eqs. (42) and (45), in the user-supplied subroutine. Thus, the continuous variation of the stiffness coefficients and thickness of the filament wound shells of revolution, along the axis of the shell, is incorporated into the free vibration analysis.

6. Effect of variation of stiffness coefficients on the free vibration characteristics

The effect of variation of stiffness coefficients on the free vibration characteristics is first studied for a truncated conical shell which has a lower end radius of 0.1 m, slant length (L) of 0.4 m and cone angle β of 30°. Each ply is assumed to be composed of high-modulus graphite epoxy with the same material properties used in the validation study. Shell wall is assumed to be composed of four layers. Filament winding angles of each layer at the narrow end of the cone is taken as [45°/−45°/45°/−45°], and each layer is assumed to have a thickness of 0.48 mm at the narrow end. The effect of the variation of the stiffness coefficients on the natural frequencies is investigated by performing solutions for the four different stiffness coefficient evaluation cases given in Table 3. In Table 3, cases C1, C2 and C3 refer to typical approximate solutions based on the assumption of constant stiffness coefficients [12].

Fig. 5 shows the variation of some of the normalized stiffness coefficients along the meridian of the truncated conical shell. Stiffness coefficients of cases C0, C1 and C2 are normalized with respect to the respective stiffness coefficients of case C3. Therefore, in Fig. 5 normalized stiffness coefficients of case C3 are of unit value. Fig. 5 shows that compared to cases C0, C1 and C2, bending stiffness coefficients (D_{ij}) and bending coupling coefficients (B_{ij}) of case C3 are substantially higher over the meridian of the cone. Case C2 is seen to provide a better average value of the stiffness coefficients for the exact stiffness coefficients given by case C0.

For each of the stiffness evaluation cases, Figs. 6 and 7 give the variation of the scaled non-dimensional fundamental natural frequency, corresponding to lateral displacement mode for the truncated conical shell, with respect to circumferential wave number. Conical shell is assumed to be clamped at the narrow end and free and clamped at the large ends, respectively. For the clamped–free case, Fig. 6 shows that at high

Table 3
Description of the different stiffness coefficient evaluation cases used in numerical studies

Cases	Description
C0	Stiffness coefficients are varied continuously along the meridian
C1	Uses average thickness from both ends of the shell, fiber orientation angle is taken from the mid length of the shell
C2	Uses thickness and fiber orientation angle from the mid length of the shell
C3	Assumes that initial thickness and winding angle is constant along the meridian of the shell

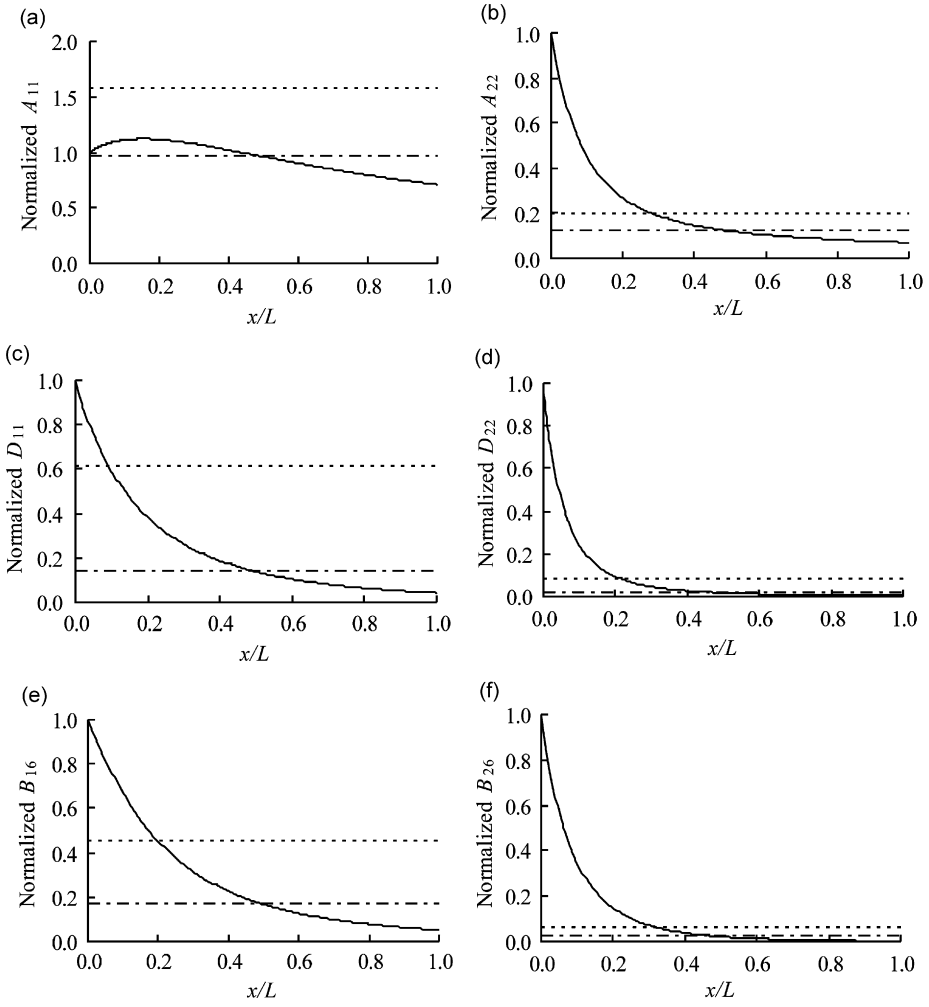

Fig. 5. Comparison of stiffness coefficients of the four different cases in Table 3 ($\beta = 30°$). *Key:* (——) C0; (- - - - - - -) C1; and (– – – – –) C2.

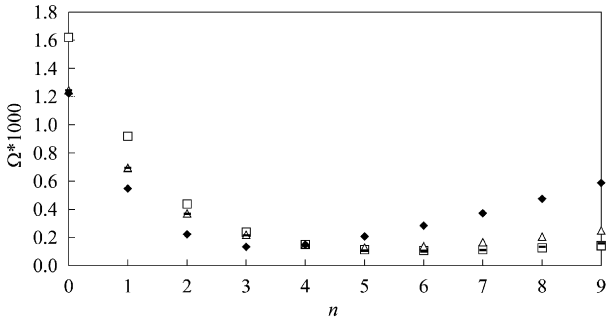

Fig. 6. Non-dimensional natural frequencies of conical shells—clamped–free case ($\beta = 30°$). *Key:* (□) C0; (△) C1; (–) C2; and (◆) C3.

circumferential wave numbers case C3 gives higher natural frequencies compared to cases C0, C1 and C2. This behavior is attributed to the dominance of bending strain energy contribution to the total strain energy at high circumferential wave numbers [22]. At high circumferential wave numbers, circumferential slices of the shell essentially behave like a longer span beam under bending. Therefore, it is seen that bending stiffness coefficient

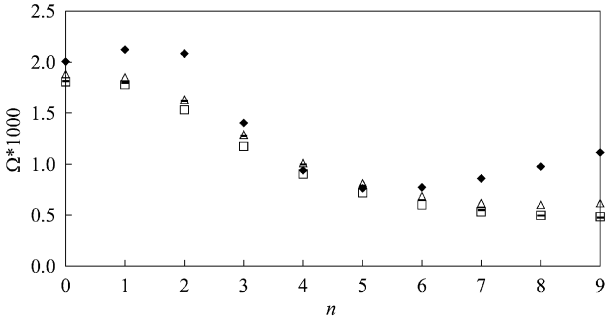

Fig. 7. Non-dimensional natural frequencies of conical shells—clamped–clamped case ($\beta = 30°$). *Key:* (□) C0; (△) C1; (–) C2; and (♦) C3.

Table 4
Comparison of non-dimensional natural frequencies ($\Omega*1000$) of conical shells; ($\beta = 30°$)

n	Clamped–free				Clamped–clamped			
	C0	C1	C2	C3	C0	C1	C2	C3
0	1.620	1.245	1.245	1.222	1.808	1.881	1.815	2.006
1	0.919	0.695	0.694	0.546	1.778	1.850	1.797	2.121
2	0.438	0.370	0.368	0.222	1.534	1.631	1.619	2.083
3	0.237	0.219	0.216	0.133	1.174	1.286	1.278	1.403
4	0.150	0.149	0.141	0.148	0.904	1.009	0.996	0.939
5	0.114	0.127	0.107	0.207	0.720	0.812	0.791	0.762
6	0.106	0.137	0.100	0.284	0.600	0.685	0.646	0.772
7	0.113	0.167	0.111	0.372	0.531	0.617	0.550	0.860
8	0.126	0.205	0.132	0.474	0.498	0.600	0.497	0.977
9	0.142	0.249	0.159	0.588	0.486	0.618	0.478	1.114

in the circumferential direction (D_{22}) predominantly governs the magnitude of the natural frequency at high circumferential wave numbers, and case C3 has the highest bending stiffness coefficient in the circumferential direction.

At low circumferential wave numbers compared to bending strain energy, the extensional strain energy is more dominant in its contribution to the total strain energy [22], and conical shell with the true representation of the stiffness coefficients (case C0) has higher natural frequencies compared to other cases. Shell with stiffness coefficients calculated based on case C3 has the lowest natural frequencies. From Fig. 5 it can be inferred that although case C3 does not have low extensional stiffness coefficients compared to other cases, the lower natural frequencies of case C3 can be attributed to the high extension–twisting coupling coefficients B_{16} and B_{26}, which effectively make the shell more flexible.

The effect of boundary conditions also becomes significant at low circumferential wave numbers. Fig. 7 shows that at low circumferential wave numbers, case C3 has higher natural frequencies contrary to the situation for the conical shell with the large end free. Fig. 5c shows that case C3 has the highest meridional bending stiffness coefficient D_{11}, and although the comparison of the cases is made for the fundamental meridional mode of vibration, it is seen that the natural frequency of the conical shell with the large end clamped is significantly affected by D_{11}. However, at high circumferential vibration modes, the bending stiffness coefficient in the circumferential direction D_{22}, again becomes the dominating factor on the fundamental natural frequencies irrespective of the boundary conditions. Table 4 summarizes the natural frequencies given in Figs. 6 and 7. It can be concluded that at high circumferential wave numbers, case C2 gives the closest natural frequencies to the natural frequencies determined by employing the actual variation of the stiffness coefficients and thickness of the shell of revolution (case C0) along the meridian of the shell of revolution. This is because, at high circumferential wave numbers bending stiffness coefficient in the

circumferential direction D_{22}, becomes the dominating factor on the natural frequencies irrespective of the boundary conditions, and case C2 gives the closest average D_{22} for the true bending stiffness coefficient in the circumferential direction. However, at low circumferential wave numbers there are significant discrepancies between the natural frequencies determined by the true modeling case C0, and approximate modeling cases C1, C2 and C3 given in Table 3.

Fig. 8 shows the variation of the scaled non-dimensional natural frequency of the truncated conical shell with respect to the cone angle for the clamped–free case and for $n = 1$. For the cylindrical shell of revolution ($\beta = 0^\circ$), Eqs. (42) and (45) show that the winding angle and thickness of filament wound cylinder does not vary along the meridian of the shell. Thus, as Fig. 8 shows, for the cylindrical shell of revolution, no difference exists among the natural frequencies determined by the four stiffness coefficient evaluation cases given in Table 3. However, for truncated conical shells of revolution, there are significant discrepancies between the natural frequencies determined by incorporating the actual variation of the stiffness coefficients along the meridian of the shell (case C0), and approximate modeling cases. Eqs. (43) and (45) show that as the cone angle is increased, the variation of the winding angle and thickness also increases, and for the initial winding angle pattern of [45°/−45°/45°/−45°], the thickness at the large end reaches its minimum value for a circular plate ($\beta = 90^\circ$). Therefore, at high cone angles natural frequencies decrease, and the absolute differences among the natural frequencies of the four cases also decrease.

The effect of different evaluation cases of the stiffness coefficients on the mode shapes is demonstrated for the conical shell, which is clamped at both edges, in Fig. 9 for $n = 1$ and cone angle of 30°. For the particular configuration, the dominant fundamental vibration mode was identified as the lateral displacement w^0. Fig. 9 shows the variation of the normalized lateral displacement with respect to the normalized slant length of the cone for the different cases described in Table 3. The actual variation of the lateral displacement over the whole conical shell can be constructed by utilizing the cosine and sine parts of the lateral displacement in the complex Fourier series representation, which is given by Eqs. (10) and (11), for $n = 1$. Fig. 9 shows that for case C3, which is based on the assumption that initial thickness and winding angle is constant along the meridian of the shell, there is a single nodal point along the meridian of the shell. However, for the other cases node disappears. Fig. 9 also shows that the mode shapes, which are determined by the approximate solutions based on the assumption of constant stiffness coefficients C1 and C2, are similar to the true mode shape determined by case C0.

By implementing the semi-analytical method of solution, a sample study is also performed for the effect of the variation of stiffness coefficients on the natural frequencies of truncated spherical shells. The truncated sphere is assumed to have a radius of 1 m, and overall thickness of 5.76 mm, and the shell is assumed to be clamped at the meridian angle of $\phi = 10^\circ$, and free at the outer edge, $\phi = 70^\circ$ (Fig. 1). Each ply is assumed to be composed of high-modulus graphite epoxy with the same material properties used in the validation study. Shell wall is assumed to be composed of four layers. Winding angles of each layer at the narrow end of the sphere are taken as [45°/−45°/45°/−45°], and each layer is assumed to have a thickness of 1.44 mm at the narrow end. For each of the stiffness evaluation cases, Fig. 10 and Table 5 give the variation of the scaled non-dimensional fundamental natural frequency, corresponding to lateral displacement mode, with respect to circumferential number. It is seen that like in conical shell, at high circumferential wave numbers case C2 gives

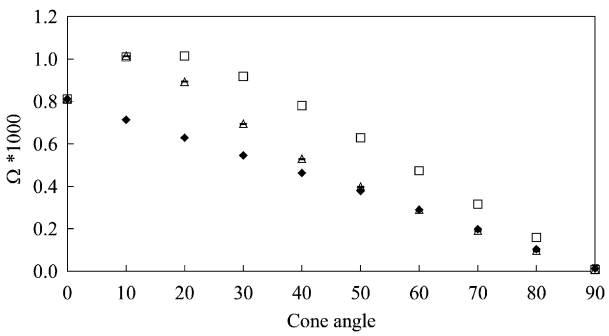

Fig. 8. Non-dimensional natural frequencies versus cone angle—clamped–free case ($n = 1$). *Key:* (□) C0; (△) C1; (–) C2; and (♦) C3.

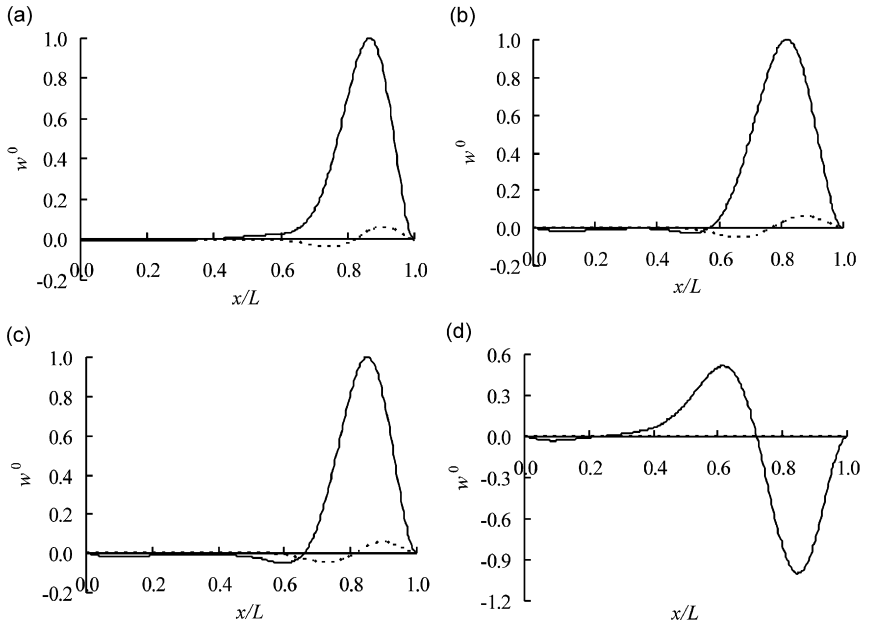

Fig. 9. Fundamental mode associated with lateral displacement (w^0); $n = 1$, $\beta = 30°$. (a) C0, (b) C1, (c) C2, and (d) C3. *Key:* (——) cosine part; (- - - - - - -) sine part.

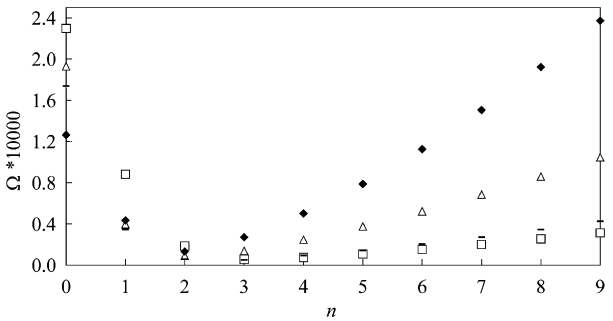

Fig. 10. Non-dimensional natural frequencies of spherical shells—clamped–free case. *Key:* (□) C0; (△) C1; (–) C2; and (♦) C3.

Table 5
Comparison of non-dimensional natural frequencies ($\Omega * 10^4$) of spherical shells

n	C0	C1	C2	C3
0	2.298	1.929	1.738	1.263
1	0.883	0.395	0.345	0.434
2	0.185	0.091	0.059	0.132
3	0.056	0.138	0.051	0.270
4	0.072	0.246	0.092	0.500
5	0.109	0.375	0.143	0.788
6	0.152	0.522	0.203	1.125
7	0.201	0.684	0.271	1.505
8	0.255	0.859	0.345	1.923
9	0.313	1.046	0.426	2.372

the best approximation to the true natural frequencies determined by case C0. However, at low circumferential wave numbers substantial differences exist between the true natural frequencies and natural frequencies determined by case C2.

7. Conclusion

In the present study, detailed description of the extension of the application of multisegment numerical integration technique to the solution of free vibration problem of filament wound anisotropic shells of revolution is presented. In the solution process, this extension is achieved by using the finite exponential Fourier transform of the fundamental system of equations, governing the free vibration of anisotropic shells of revolution, through the use of a modified frequency trial method.

For the filament wound shells of revolution, filaments are assumed to be placed along the geodesic fiber path on the shell of revolution resulting in the variation of the stiffness coefficients along the axis of the shell of revolution with general meridional curvature. Therefore, the variation of the stiffness coefficients along the axis of the shell is also incorporated into the semi-analytical solution method. Sample studies on the effect of variation of the stiffness coefficients on the free vibration characteristics have been performed for truncated conical and spherical shells of revolution. Comparison of the fundamental natural frequencies, which are obtained by the typical approximate solutions based on the assumption of constant stiffness coefficients, with the true fundamental natural frequencies, calculated by incorporating the continuous variation of the stiffness coefficients, show that there exist substantial differences among the natural frequencies. At high circumferential wave numbers, the approximate stiffness coefficient evaluation case C2, which uses thickness and fiber orientation angle from the mid length of the shell, gives the best approximation to the true natural frequencies.

It is concluded that the free vibration analysis of filament wound shells of revolution should be performed by incorporating the actual variation of the stiffness coefficients. The differences between the fundamental natural frequencies determined by the approximate methods, based on constant stiffness coefficients, and true natural frequencies are not negligible for the free vibration and dynamic loading problems involving filament wound shells of revolution.

Appendix A

For a general shell of revolution, elements of the coefficient matrix in Eq. (14) are given below

$$\mathbf{K}=\begin{bmatrix}\mathbf{K}_{11} & . & . & \mathbf{K}_{110}\\ . & . & . & .\\ . & . & . & .\\ \mathbf{K}_{101} & . & . & \mathbf{K}_{1010}\end{bmatrix}_{20\times 20} \tag{A.1}$$

$$\mathbf{K}_{11}=\{0/ncp_{11}\};\ \mathbf{K}_{12}=\{c_{12}/0\};\ \mathbf{K}_{13}=\{c_{13}/0\};\ \mathbf{K}_{14}=\{c_{14}/0\};\ \mathbf{K}_{15}=\{c_{15}/0\};$$
$$\mathbf{K}_{16}=\{c_{16}/0\};\ \mathbf{K}_{17}=\{0/0\};\ \mathbf{K}_{18}=\{0/0\};\ \mathbf{K}_{19}=\{0/0\};\ \mathbf{K}_{110}=\{0/0\} \tag{A.2}$$

$$\mathbf{K}_{21}=\{c_{21}/0\};\ \mathbf{K}_{22}=\{c_{22}/ncp_{22}\};\ \mathbf{K}_{23}=\{c_{23}/ncp_{23}\};\ \mathbf{K}_{24}=\{c_{24}/ncp_{24}\};\ \mathbf{K}_{25}=\{c_{25}/ncp_{25}\};$$
$$\mathbf{K}_{26}=\{0/0\};\ \mathbf{K}_{27}=\{c_{27}/0\};\ \mathbf{K}_{28}=\{c_{28}/0\};\ \mathbf{K}_{29}=\{c_{29}/0\};\ \mathbf{K}_{210}=\{c_{210}/0\} \tag{A.3}$$

$$\mathbf{K}_{31}=\{c_{31}/0\};\ \mathbf{K}_{32}=\{c_{32}/ncp_{32}\};\ \mathbf{K}_{33}=\{c_{33}/ncp_{33}\};\ \mathbf{K}_{34}=\{c_{34}/ncp_{34}\};\ \mathbf{K}_{35}=\{c_{35}/ncp_{35}\};$$
$$\mathbf{K}_{36}=\{0/0\};\ \mathbf{K}_{37}=\{c_{37}/0\};\ \mathbf{K}_{38}=\{c_{38}/0\};\ \mathbf{K}_{39}=\{c_{39}/0\};\ \mathbf{K}_{310}=\{c_{310}/0\} \tag{A.4}$$

$$\mathbf{K}_{41}=\{c_{41}/0\};\ \mathbf{K}_{42}=\{c_{42}/ncp_{42}\};\ \mathbf{K}_{43}=\{c_{43}/ncp_{43}\};\ \mathbf{K}_{44}=\{c_{44}/ncp_{44}\};\ \mathbf{K}_{45}=\{c_{45}/ncp_{45}\};$$
$$\mathbf{K}_{46}=\{0/0\};\ \mathbf{K}_{47}=\{c_{47}/0\};\ \mathbf{K}_{48}=\{c_{48}/0\};\ \mathbf{K}_{49}=\{c_{49}/0\};\ \mathbf{K}_{410}=\{c_{410}/0\} \tag{A.5}$$

$$\mathbf{K}_{51}=\{c_{51}/0\};\ \mathbf{K}_{52}=\{c_{52}/ncp_{52}\};\ \mathbf{K}_{53}=\{c_{53}/ncp_{53}\};\ \mathbf{K}_{54}=\{c_{54}/ncp_{54}\};\ \mathbf{K}_{55}=\{c_{55}/ncp_{55}\};$$
$$\mathbf{K}_{56}=\{0/0\};\ \mathbf{K}_{57}=\{c_{57}/0\};\ \mathbf{K}_{58}=\{c_{58}/0\};\ \mathbf{K}_{59}=\{c_{59}/0\};\ \mathbf{K}_{510}=\{c_{510}/0\} \tag{A.6}$$

$$\mathbf{K}_{61}=\begin{Bmatrix} c_{61} \\ -n^2 cdp_{61}/0 \end{Bmatrix};\ \mathbf{K}_{62}=\{c_{62}/ncp_{62}\};\ \mathbf{K}_{63}=\{c_{63}/ncp_{63}\};\ \mathbf{K}_{64}=\{c_{64}/ncp_{64}\};\mathbf{K}_{65}=\{c_{65}/ncp_{65}\};$$
$$\mathbf{K}_{66}=\{c_{66}/ncp_{66}\};\ \mathbf{K}_{67}=\{c_{67}/0\};\ \mathbf{K}_{68}=\{c_{68}/0\};\ \mathbf{K}_{69}=\{c_{69}/0\};\ \mathbf{K}_{610}=\{c_{610}/0\} \tag{A.7}$$

$$\mathbf{K}_{71}=\{c_{71}/0\};\ \mathbf{K}_{72}=\{c_{72}/ncp_{72}\};\ \mathbf{K}_{73}=\{c_{73}/ncp_{73}\};\ \mathbf{K}_{74}=\{c_{74}/ncp_{74}\};\ \mathbf{K}_{75}=\{c_{75}/ncp_{75}\};$$
$$\mathbf{K}_{76}=\{c_{76}/0\};\ \mathbf{K}_{77}=\{c_{77}/0\};\ \mathbf{K}_{78}=\{c_{78}/ncp_{78}\};\ \mathbf{K}_{79}=\{c_{79}/0\};\ \mathbf{K}_{710}=\{c_{710}/0\} \tag{A.8}$$

$$\mathbf{K}_{81}=\{0/ncp_{81}\};\ \mathbf{K}_{82}=\begin{Bmatrix} c_{82}-n^2 cdp_{82} \\ /ncp_{82} \end{Bmatrix};\ \mathbf{K}_{83}=\begin{Bmatrix} c_{83}-n^2 cdp_{83} \\ /ncp_{83} \end{Bmatrix};\ \mathbf{K}_{84}=\begin{Bmatrix} c_{84}-n^2 cdp_{84} \\ /ncp_{84} \end{Bmatrix};$$
$$\mathbf{K}_{85}=\begin{Bmatrix} c_{85}-n^2 cdp_{85} \\ /ncp_{85} \end{Bmatrix};\mathbf{K}_{86}=\{c_{86}/0\};\ \mathbf{K}_{87}=\{0/ncp_{87}\};\ \mathbf{K}_{88}=\{c_{88}/ncp_{88}\};\ \mathbf{K}_{89}=\{0/ncp_{89}\};$$
$$\mathbf{K}_{810}=\{0/ncp_{810}\} \tag{A.9}$$

$$\mathbf{K}_{91}=\{c_{91}/0\};\ \mathbf{K}_{92}=\{c_{92}/ncp_{92}\};\ \mathbf{K}_{93}=\{c_{93}/ncp_{93}\};\ \mathbf{K}_{94}=\{c_{94}/ncp_{94}\};\ \mathbf{K}_{95}=\{c_{95}/ncp_{95}\};$$
$$\mathbf{K}_{96}=\{c_{96}/0\};\ \mathbf{K}_{97}=\{c_{97}/0\};\ \mathbf{K}_{98}=\{c_{98}/0\};\ \mathbf{K}_{99}=\{c_{99}/0\};\ \mathbf{K}_{910}=\{c_{910}/ncp_{910}\} \tag{A.10}$$

$$\mathbf{K}_{101}=\{0/ncp_{101}\};\ \mathbf{K}_{102}=\begin{Bmatrix} c_{102}-n^2 cdp_{102} \\ /ncp_{102} \end{Bmatrix};\ \mathbf{K}_{103}=\begin{Bmatrix} c_{103}-n^2 cdp_{103} \\ /ncp_{103} \end{Bmatrix};\ \mathbf{K}_{104}=\begin{Bmatrix} c_{104}-n^2 cdp_{104} \\ /ncp_{104} \end{Bmatrix};$$
$$\mathbf{K}_{105}=\begin{Bmatrix} c_{105}-n^2 cdp_{105} \\ /ncp_{105} \end{Bmatrix};\ \mathbf{K}_{106}=\{c_{106}/0\};\ \mathbf{K}_{107}=\{0/ncp_{107}\};\ \mathbf{K}_{108}=\{0/ncp_{108}\};\ \mathbf{K}_{109}=\{0/ncp_{109}\};$$
$$\mathbf{K}_{1010}=\{c_{1010}/ncp_{1010}\} \tag{A.11}$$

In $\{a/b\}$ notation, a and b refer to the diagonal, and off-diagonal elements of the 2×2 matrices, respectively, and $\{a/b\}$ is defined by

$$\{a/b\}=\begin{bmatrix} a & b \\ -b & a \end{bmatrix} \tag{A.12}$$

The coefficients appearing in the **K** matrix are given below.

$$cp_{11}=-\frac{R_\phi As_{45}}{R_\theta \sin\phi As_{55}};\ c_{12}=1;\ c_{13}=\frac{R_\phi As_{45}}{R_\theta As_{55}};\ c_{14}=-R_\phi;\ c_{15}=-\frac{As_{45}R_\phi}{As_{55}};\ c_{16}=\frac{R_\phi}{As_{55}} \tag{A.13}$$

$$c_{k1}=(1/\Delta)\{(-1/R_\phi)[A_{11}Z_1^k+A_{16}Z_2^k+B_{11}Z_3^k+B_{16}Z_4^k]-(1/R_\theta)[A_{12}Z_1^k+A_{26}Z_2^k+B_{12}Z_3^k+B_{26}Z_4^k]\}$$
$$c_{k2}=(1/\Delta)(-\cot\phi/R_\theta)\{A_{12}Z_1^k+A_{26}Z_2^k+B_{12}Z_3^k+B_{26}Z_4^k\}$$
$$cp_{k2}=(1/\Delta)(-1/R_\theta\sin\phi)\{A_{16}Z_1^k+A_{66}Z_2^k+B_{16}Z_3^k+B_{66}Z_4^k\}$$
$$c_{k3}=(1/\Delta)(\cot\phi/R_\theta)\{A_{16}Z_1^k+A_{66}Z_2^k+B_{16}Z_3^k+B_{66}Z_4^k\}$$

$$
\begin{aligned}
cp_{k3} &= (1/\Delta)(-1/R_\theta \sin\phi)\{A_{12}Z_1^k + A_{26}Z_2^k + B_{12}Z_3^k + B_{26}Z_4^k\}\\
c_{k4} &= (1/\Delta)(-\cot\phi/R_\theta)\{B_{12}Z_1^k + B_{26}Z_2^k + D_{12}Z_3^k + D_{26}Z_4^k\}\\
cp_{k4} &= (1/\Delta)(-1/R_\theta \sin\phi)\{B_{16}Z_1^k + B_{66}Z_2^k + D_{16}Z_3^k + D_{66}Z_4^k\}\\
c_{k5} &= (1/\Delta)(\cot\phi/R_\theta)\{B_{16}Z_1^k + B_{66}Z_2^k + D_{16}Z_3^k + D_{66}Z_4^k\}\\
cp_{k5} &= (1/\Delta)(-1/R_\theta \sin\phi)\{B_{12}Z_1^k + B_{26}Z_2^k + D_{12}Z_3^k + D_{26}Z_4^k\}\\
c_{k7} &= Z_1^k/\Delta;\ \ c_{k8} = Z_2^k/\Delta;\ \ c_{k9} = Z_3^k/\Delta;\ \ c_{k10} = Z_4^k/\Delta
\end{aligned}
\tag{A.14}
$$

where $k = 2$–5

$$
\begin{aligned}
Z_1^2 &= A_{66}D_{11}D_{66} - A_{66}D_{16}^2 - D_{66}B_{16}^2 + 2B_{16}B_{66}D_{16} - D_{11}B_{66}^2\\
Z_2^2 &= -A_{16}D_{11}D_{66} + A_{16}D_{16}^2 + B_{16}B_{11}D_{66} - D_{16}B_{16}^2 - B_{66}B_{11}D_{16} + B_{66}B_{16}D_{11}\\
Z_3^2 &= A_{16}B_{16}D_{66} - A_{16}B_{66}D_{16} - A_{66}B_{11}D_{66} + A_{66}B_{16}D_{16} + B_{11}B_{66}^2 - B_{66}B_{16}^2\\
Z_4^2 &= -A_{16}B_{16}D_{16} + A_{16}B_{66}D_{11} + A_{66}B_{11}D_{16} - A_{66}B_{16}D_{11} - B_{16}B_{11}B_{66} + B_{16}^3
\end{aligned}
\tag{A.15}
$$

$$
\begin{aligned}
Z_1^3 &= -A_{16}D_{11}D_{66} + A_{16}D_{16}^2 + B_{11}B_{16}D_{66} - B_{11}B_{66}D_{16} - D_{16}B_{16}^2 + B_{16}B_{66}D_{11}\\
Z_2^3 &= A_{11}D_{11}D_{66} - A_{11}D_{16}^2 - D_{66}B_{11}^2 + 2B_{11}B_{16}D_{16} - D_{11}B_{16}^2\\
Z_3^3 &= -A_{11}B_{16}D_{66} + A_{11}B_{66}D_{16} + A_{16}B_{11}D_{66} - A_{16}B_{16}D_{16} - B_{16}B_{11}B_{66} + B_{16}^3\\
Z_4^3 &= A_{11}B_{16}D_{16} - A_{11}B_{66}D_{11} - A_{16}B_{11}D_{16} + A_{16}B_{16}D_{11} + B_{66}B_{11}^2 - B_{11}B_{16}^2
\end{aligned}
\tag{A.16}
$$

$$
\begin{aligned}
Z_1^4 &= A_{16}B_{16}D_{66} - A_{16}D_{16}B_{66} - B_{11}A_{66}D_{66} + B_{11}B_{66}^2 + B_{16}A_{66}D_{16} - B_{66}B_{16}^2\\
Z_2^4 &= -A_{11}B_{16}D_{66} + A_{11}D_{16}B_{66} + B_{11}A_{16}D_{66} - B_{11}B_{16}B_{66} - B_{16}A_{16}D_{16} + B_{16}^3\\
Z_3^4 &= A_{11}A_{66}D_{66} - A_{11}B_{66}^2 - D_{66}A_{16}^2 + 2A_{16}B_{16}B_{66} - A_{66}B_{16}^2\\
Z_4^4 &= -A_{11}A_{66}D_{16} + A_{11}B_{66}B_{16} + D_{16}A_{16}^2 - A_{16}B_{16}^2 - B_{11}A_{16}B_{66} + B_{11}B_{16}A_{66}
\end{aligned}
\tag{A.17}
$$

$$
\begin{aligned}
Z_1^5 &= -A_{16}B_{16}D_{16} + A_{16}D_{11}B_{66} + B_{11}A_{66}D_{16} - B_{11}B_{16}B_{66} - B_{16}A_{66}D_{11} + B_{16}^3\\
Z_2^5 &= A_{11}B_{16}D_{16} - A_{11}D_{11}B_{66} - B_{11}A_{16}D_{16} + B_{66}B_{11}^2 + B_{16}A_{16}D_{11} - B_{11}B_{16}^2\\
Z_3^5 &= -A_{11}A_{66}D_{16} + A_{11}B_{16}B_{66} + D_{16}A_{16}^2 - A_{16}B_{11}B_{66} - A_{16}B_{16}^2 + B_{16}B_{11}A_{66}\\
Z_4^5 &= A_{11}A_{66}D_{11} - A_{11}B_{16}^2 - D_{11}A_{16}^2 + 2A_{16}B_{11}B_{16} - A_{66}B_{11}^2
\end{aligned}
\tag{A.18}
$$

$$
\Delta = \frac{1}{R_\phi}\begin{bmatrix}
A_{11}A_{66}D_{11}D_{66} - A_{11}A_{66}D_{16}^2 - A_{11}D_{66}B_{16}^2 + 2A_{11}B_{16}B_{66}D_{16} - A_{11}D_{11}B_{66}^2 - D_{11}D_{66}A_{16}^2\\
+A_{16}^2D_{16}^2 + 2A_{16}B_{16}B_{11}D_{66} - 2A_{16}D_{16}B_{16}^2 - 2A_{16}B_{66}B_{11}D_{16} + 2A_{16}B_{66}B_{16}D_{11} - A_{66}D_{66}B_{11}^2\\
+2A_{66}B_{11}B_{16}D_{16} + B_{11}^2B_{66}^2 - 2B_{11}B_{66}B_{16}^2 - B_{16}A_{66}B_{16}D_{11} + B_{16}^4
\end{bmatrix}
\tag{A.19}
$$

$$
\begin{aligned}
c_{6m} = &-(\rho h\omega^2 R_\phi)^{(+1)} + \left(\frac{R_\phi A_{22}}{R_\theta^2}\right)^{(+1)} + \frac{1}{R_\theta}\left[A_{12}c_{2m} + A_{26}c_{3m} + B_{12}c_{4m} + B_{26}c_{5m} + (A_{12})^{(+1)}\right]\\
&+\cot\phi\,\frac{R_\phi}{R_\theta^2}\left[(A_{22})^{(+2)} - (A_{26})^{(+3)} + (B_{22})^{(+4)} - (B_{26})^{(+5)}\right] + (1)^{(+7)} \quad (m = 1{-}5,\ 7{-}10)
\end{aligned}
\tag{A.20}
$$

$$
c_{66} = -\frac{R_\phi}{R_\theta}\cot\phi \tag{A.21}
$$

$$cp_{6m}=\frac{1}{R_\theta}\left[-\frac{As_{45}c_{1m}}{\sin\ \phi}+A_{12}cp_{2m}+A_{26}cp_{3m}+B_{12}cp_{4m}+B_{26}cp_{5m}+\left(\frac{As_{45}}{\sin\ \phi}\right)^{(+2)}+\left(\frac{R_\phi As_{44}}{R_\theta\ \sin\ \phi}\right)^{(+3)}-\left(\frac{R_\phi As_{45}}{\sin\ \phi}\right)^{(+4)}-\left(\frac{R_\phi As_{44}}{\sin\ \phi}\right)^{(+5)}+\frac{R_\phi}{R_\theta\ \sin\ \phi}\left\{(A_{26})^{(+2)}+(A_{22})^{(+3)}+(B_{26})^{(+4)}+(B_{22})^{(+5)}\right\}\right]\quad(m=2-5)\tag{A.22}$$

$$cp_{66}=\frac{-As_{45}c_{16}}{R_\theta\ \sin\ \phi}\tag{A.23}$$

$$c\mathrm{d}p_{61}=-\frac{As_{45}cp_{11}}{R_\theta\ \sin\ \phi}-\frac{R_\phi As_{44}}{R_\theta^2\sin^2\phi}\tag{A.24}$$

$$c_{7m}=\frac{\cot\ \phi}{R_\theta}\left[A_{12}c_{2m}+A_{26}c_{3m}+B_{12}c_{4m}+B_{26}c_{5m}+(A_{12})^{(+1)}+\left(\frac{R_\phi A_{22}}{R_\theta}\right)^{(+1)}-(R_\phi)^{(+7)}\right]+\frac{R_\phi\cot^2\phi}{R_\theta^2}\left[(A_{22})^{(+2)}-(A_{26})^{(+3)}+(B_{22})^{(+4)}-(B_{26})^{(+5)}\right]-(\rho h\omega^2R_\phi)^{(+2)}\quad(m=1-5,7-10)\tag{A.25}$$

$$c_{76}=-1\tag{A.26}$$

$$cp_{7m}=\frac{\cot\ \phi}{R_\theta}\left[A_{12}cp_{2m}+A_{26}cp_{3m}+B_{12}cp_{4m}+B_{26}cp_{5m}+\frac{R_\phi}{R_\theta\ \sin\ \phi}\left\{(A_{26})^{(+2)}+(A_{22})^{(+3)}+(B_{26})^{(+4)}+(B_{22})^{(+5)}\right\}\right]\quad(m=2-5)\tag{A.27}$$

$$cp_{78}=-\frac{R_\phi}{R_\theta\ \sin\ \phi}\tag{A.28}$$

$$c_{8m}=\frac{1}{R_\theta}\left[-As_{45}c_{1m}+(As_{45})^{(+2)}+\left(\frac{R_\phi As_{44}}{R_\theta}\right)^{(+3)}-(R_\phi As_{45})^{(+4)}-(R_\phi As_{44})^{(+5)}\right]-(\rho h\omega^2R_\phi)^{(+3)}\quad(m=2-6)\tag{A.29}$$

$$c_{88}=\frac{-2R_\phi}{R_\theta}\cot\ \phi\tag{A.30}$$

$$cp_{8m}=\frac{-1}{R_\theta\ \sin\ \phi}\left[A_{12}c_{2m}+A_{26}c_{3m}+B_{12}c_{4m}+B_{26}c_{5m}+(A_{12})^{(+1)}+\left(\frac{R_\phi A_{22}}{R_\theta}\right)^{(+1)}\right]+\frac{R_\phi\ \cot\ \phi}{R_\theta^2\ \sin\ \phi}\left[-(A_{22})^{(+2)}+(A_{26})^{(+3)}-(B_{22})^{(+4)}+(B_{26})^{(+5)}\right]-\left[\frac{As_{45}}{R_\theta}cp_{11}+\frac{R_\phi As_{44}}{R_\theta^2\ \sin\ \phi}\right]^{(+1)}\quad(m=1-5,7-10)\tag{A.31}$$

$$c\mathrm{d}p_{8m}=\frac{-1}{R_\theta\ \sin\ \phi}\left[A_{12}cp_{2m}+A_{26}cp_{3m}+B_{12}cp_{4m}+B_{26}cp_{5m}+\frac{R_\phi}{R_\theta\ \sin\ \phi}\left\{(A_{26})^{(+2)}+(A_{22})^{(+3)}+(B_{26})^{(+4)}+(B_{22})^{(+5)}\right\}\right]\quad(m=2-5)\tag{A.32}$$

$$c_{9m} = \frac{\cot\phi}{R_\theta}\left[B_{12}c_{2m} + B_{26}c_{3m} + D_{12}c_{4m} + D_{26}c_{5m} + (B_{12})^{(+1)} + \left(\frac{R_\phi B_{22}}{R_\theta}\right)^{(+1)} - (R_\phi)^{(+9)}\right] + \frac{R_\phi \cot^2\phi}{R_\theta^2}\left[(B_{22})^{(+2)} - (B_{26})^{(+3)} + (D_{22})^{(+4)} - (D_{26})^{(+5)}\right] - \left(\frac{1}{12}\rho h^3\omega^2 R_\phi\right)^{(+4)} \quad (m = 1-5, 7-10) \tag{A.33}$$

$$c_{96} = R_\phi \tag{A.34}$$

$$cp_{9m} = \frac{\cot\phi}{R_\theta}\left[B_{12}cp_{2m} + B_{26}cp_{3m} + D_{12}cp_{4m} + D_{26}cp_{5m} + \frac{R_\phi}{R_\theta \sin\phi}\left\{(B_{26})^{(+2)} + (B_{22})^{(+3)} + (D_{26})^{(+4)} + (D_{22})^{(+5)}\right\}\right] \quad (m = 2-5) \tag{A.35}$$

$$cp_{910} = -\frac{R_\phi}{R_\theta \sin\phi} \tag{A.36}$$

$$c_{10m} = As_{45}c_{1m} - (As_{45})^{(+2)} - \left(\frac{R_\phi As_{44}}{R_\theta}\right)^{(+3)} + R_\phi\left\{(As_{45})^{(+4)} + (As_{44})^{(+5)}\right\} - \left(\frac{1}{12}\rho h^3\omega^2 R_\phi\right)^{(+5)} \quad (m = 2-6) \tag{A.37}$$

$$c_{1010} = \frac{-2R_\phi}{R_\theta}\cot\phi \tag{A.38}$$

$$cp_{10m} = \frac{-1}{R_\theta \sin\phi}\left[B_{12}c_{2m} + B_{26}c_{3m} + D_{12}c_{4m} + D_{26}c_{5m} + (B_{12})^{(+1)} + \left(\frac{R_\phi B_{22}}{R_\theta}\right)^{(+1)}\right] + \frac{R_\phi \cot\phi}{R_\theta^2 \sin\phi}\left[-(B_{22})^{(+2)} + (B_{26})^{(+3)} - (D_{22})^{(+4)} + (D_{26})^{(+5)}\right] + \left(As_{45}cp_{11} + \frac{R_\phi As_{44}}{R_\theta \sin\phi}\right)^{(+1)} \quad (m = 1-5, 7-10) \tag{A.39}$$

$$cdp_{10m} = \frac{-1}{R_\theta \sin\phi}\left[B_{12}cp_{2m} + B_{26}cp_{3m} + D_{12}cp_{4m} + D_{26}cp_{5m} + \frac{R_\phi}{R_\theta \sin\phi}\left\{(B_{26})^{(+2)} + (B_{22})^{(+3)} + (D_{26})^{(+4)} + (D_{22})^{(+5)}\right\}\right] \quad (m = 2-5) \tag{A.40}$$

In the expressions for the coefficients given above, the terms with $(\ )^{(+m)}$ should be included in the relevant coefficient with the same subscript "m". For instance, when $m = 1$ the term $(-\rho h\omega^2 R_\phi)^{(+1)}$ should be included in the coefficient c_{61}. Terms without any superscript $(+m)$ should be included in all coefficients with subscript m.

References

[1] A.K. Noor, W.S. Burton, Assessment of computational models for multilayered composite shells, *Applied Mechanics Reviews* 43 (1990) 67–97.

[2] A.K. Noor, J.M. Peters, Vibration analysis of laminated anisotropic shells of revolutions, *Computer Methods in Applied Mechanics and Engineering* 61 (1987) 277–301.

[3] N. Ganesan, K.R. Sivadas, Effect of coupling between in-plane strains and twist due to anisotropy on vibrations of composite shells, *Computers and Structures* 49 (1993) 481–493.

[4] I. Sheinman, S. Weissman, Coupling between symmetric and antisymmetric modes in shells of revolution, *Journal of Composite Materials* 21 (1987) 988–1007.

[5] Z.C. Xi, L.H. Yam, T.P. Leung, Semi-analytical study of free vibration of composite shells of revolution based on the Reissner–Mindlin assumption, *International Journal of Solids and Structures* 33 (1996) 851–863.
[6] I.F. Pinto Correia, J.I. Barbosa, C.M. Mota Soares, C.A. Mota Soares, A finite element semi-analytical model for laminated axisymmetric shells: statics, dynamics and buckling, *Computers and Structures* 76 (2000) 299–317.
[7] P.R. Heyliger, A. Jilani, Free vibrations of laminated anisotropic cylindrical shells, *Journal of Engineering Mechanics* 119 (1993) 1062–1077.
[8] D.Y. Tan, Free vibration analysis of shells of revolution, *Journal of Sound and Vibration* 213 (1998) 15–33.
[9] T. Tımarcı, K.P. Soldatos, Vibrations of angle-ply laminated circular cylindrical shells subjected to different sets of edge boundary conditions, *Journal of Engineering Mathematics* 37 (2000) 211–230.
[10] A. Kalnins, Free vibration of rotationally symmetric shells, *Journal of the Acoustical Society of America* 36 (1964) 1355–1365.
[11] A. Kayran, E. Yavuzbalkan, Numerical integration based vibration analysis of anisotropic branched shells of revolution with ring stiffeners, *AIAA-2007-2114, 48th AIAA/ASME/ASCE/AHS/ASC Structures, Structural Dynamics, and Materials Conference*, Honolulu, Hawaii, April 23–26, 2007.
[12] Y. Goldfeld, J. Arbocz, Buckling of laminated conical shells given the variations of the stiffness coefficients, *AIAA Journal* 42 (2004) 642–649.
[13] W. Soedel, *Vibration of Shells and Plates*, Marcel Dekker, New York, 1993.
[14] J.R. Vinson, R.L. Sierakowski, *The Behaviour of Structures Composed of Composite Materials*, second ed., Kluwer Academic Publishers, Dordrecht, The Netherlands, 2002.
[15] M.H. Toorani, A.A. Lakis, General equations of anisotropic plates and shells including transverse shear deformations, rotatory inertia and initial curvature effects, *Journal of Sound and Vibration* 237 (2000) 561–615.
[16] E. Reissner, A new derivation of the equations for the deformation of elastic shells, *American Journal of Mathematics* 63 (1941) 177–184.
[17] J.M. Whitney, The effect of transverse shear deformation on the bending of laminated plates, *Journal of Composite Materials* 3 (1969) 534–547.
[18] R.D. Mindlin, Influence of rotatory inertia and shear on flexural motions of isotropic, elastic plates, *Journal of Applied Mechanics* 18 (1951) 31–38.
[19] E. Yavuzbalkan, Free Vibration Analysis of Anisotropic Laminated Composite Shells of Revolution, MSc Thesis, Department of Aerospace Engineering, Middle East Technical University, 2005.
[20] A. Kayran, J.R. Vinson, Free vibration analysis of laminated composite truncated circular conical shells, *AIAA Journal* 28 (1990) 1259–1269.
[21] J.S. Park, C.S. Hong, C.G. Kim, C.U. Kim, Analysis of filament wound composite structures considering the change of winding angles through the thickness direction, *Composite Structures* 55 (2002) 63–71.
[22] R.N. Arnold, G.B. Warburton, Flexural vibrations of the walls of thin cylindrical shells having freely supported ends, *Proceedings of the Royal Society of London, Series A, Mathematical and Physical Sciences* 197 (1949) 238–256.